University of Tartu
Faculty of Science and Technology
Institute of Physics

Kristiina Verro

Physical Properties of the Nova Remnant Nova Persei 1901

Bachelor's thesis

Supervisors:
MSc Tiina Liimets
PhD Romano L. M. Corradi

Tartu 2015

Contents

1 Introduction

Nova Persei 1901 (also called GK Persei or GK Per for short), being a classical nova, is a binary system with a white dwarf and an evolved late-type star. Late-type stars are cooler and less massive than our Sun (Moore & Rees 2011, p. 262-263). The evolved star is overflowing its Roche lobe, the space around the star where matter is gravitationally bound to the star, and losing mass to the white dwarf's lobe. The inflowing mass forms an accretion disc around the white dwarf. Hydrogen-rich material builds up onto the surface of the white dwarf, thus rising the temperature until it becomes high enough (10^7 K) to start a runaway thermonuclear reactions that lead to a nova outburst. This is a violent process, the expansion velocity of the shell is usually in the order of 10^3 km/s, but the system returns to the original state, because the event is not energetic enough to destroy the binary star. The overflow and accretion of matter can continue, so nova explosion can reoccur. After the outburst and peak luminosity, the shell increases in size and decreases in density and luminosity; this should happen in a uniform rate, but often does not (Osterbrock & Ferland 2006, p. 295-296). The geometry and physics of the ejection of stellar matter is not well understood – stars are symmetric, but the ejecta are often asymmetric.

This thesis is part of a study of the evolution of stellar outflow of GK Persei, which in turn is part of an international project (led by R.Corradi) that investigates the structure and kinematics of circumstellar matter around typical representatives of outbursting stellar objects (V838 Mon, GK Persei and R Aquarii). Nova Persei 1901 was chosen for this study because it is the longest visible nova remnant and also one of the most energetic classical nova remnants – it is expanding and evolving in human timescales. The star was discovered on 21st of February 1901 by Scottish clergyman Thomas David Anderson, when it had brightened up from fainter than 12th to a 2.7 magnitude star. Brightness reached maximum in a few days, with 0.3 magnitude, comparable with the star Vega (Pickering 1901). The ejecta itself became visible 15 years later, an was discovered by Barnard (1916). GK Per is one of the most observed and studied nova shells.

The first objective of this thesis was to perform proper motion and flux evolution measurements on optical photometric images of the nova shell. 19 images were taken between 2004–2011 with The Isaac Newton Telescope (INT[1]) and The Nordic Optical Telescope (NOT)[2]. To get additional information about the acceleration or

[1]The Isaac Newton Telescope is operated by the Isaac Newton Group at the Observatorio del Roque de los Muchachos, La Palma, Spain of the Instituto de Astrofisica de Canarias

[2]Nordic Optical Telescope is operated by the Nordic Optical Telescope Association at the Observatorio del Roque de los Muchachos, La Palma, Spain, of the Instituto de Astrofisica de Canarias

deceleration of the nova shell, additional measurements were done on five archival images from various telescopes, from which the earliest dates back to 1987. Measurements done for this thesis have given data with great scientific value and has resulted in a scientific paper published in The Astrophysical Journal: *A 3D view of the remnant of Nova Persei 1901 (GK Per)* (Liimets et al. 2012).

The second purpose of this thesis was to go further with the analysis of the nova shell, by determining the electron temperature inside the nova shell, which is one of the key parameters in characterizing a remnant. A long-slit spectrum of a part of the remnant was acquired with NOT. The task was to perform standard data reduction and calibration on the spectrum, to extract one-dimensional spectra of the gas clumps of the remnant from the long-slit spectrum and to analyse the strengths of emission lines of certain elements to find electron temperature inside the clumps.

2 Imaging of the nova remnant Nova Persei 1901

2.1 Morphology of the remnant

After the nova outburst, the ejecta is dense and optically thick for wavelengths from ultraviolet to infrared (Osterbrock & Ferland 2006, p. 295-296). After reaching its maximum luminosity, the shell becomes less dense and optically thin; meanwhile, the shell increases in size and decreases in luminosity. Finally, the remnant becomes fainter until disappearing, becoming one with the interstellar medium.

The evolution of Nova Persei 1901 is observable in human timescales. At present, the optical remnant has a round morphology, with seemingly small deviation from the symmetry: diameter on Figure 1 is in the North-East–South-West direction (95") slightly smaller (roughly 13") than in the across direction (108"). The ejecta of GK Persei consists of gaseous filaments, or "knots". The knots differ in sizes and brightnesses and some form larger elongated filaments pointing towards the central star; a jet-like feature is also present in the North-East quadrant (can be seen on Figure 5). Furthermore, an hourglass-shaped faint optical nebulosity extending greatly beyond the nova ejecta was discovered by Tweedy (1995). It is believed to be an ancient nebula, connected to the binary's earlier evolution (Bode et al. 2004).

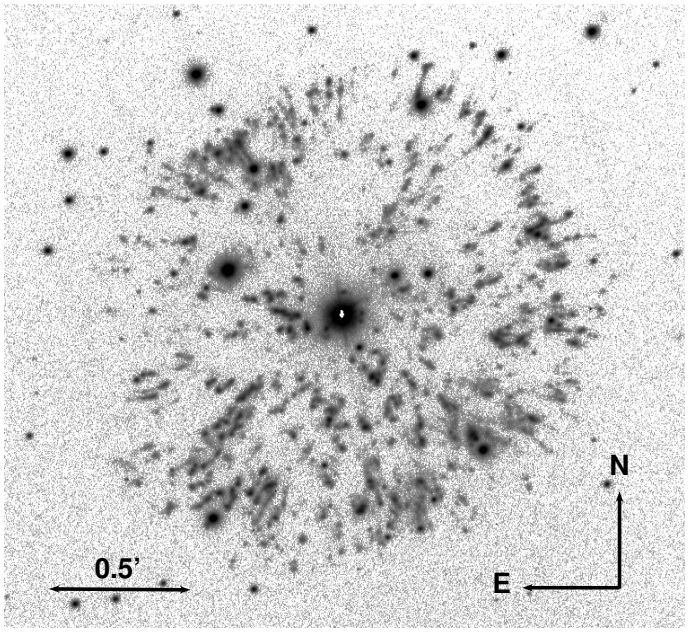

Figure 1: GK Persei narrowband Hα image taken with NOT, 2007-09-04.

The morphology of a remnant is dependent on the wavelength band which the remnant is viewed in. In our photometric study, Hα(6568, 6577 Å) and [NII](6590 Å)

narrowband filters were used, as described in Section 2.2 and Table 1. Although GK Persei is quite round on Figure 1, the object is well known to be highly asymmetric. The early optical images taken of GK Persei showed emission only in the South-West region. Radio observations show non-thermal emission caused by electron acceleration in the South-West region. Also, images in X-ray show an asymmetric remnant only in the South-West region (Bode et al. 2004, and references therein; Takei et al. 2015). Bode et al. (2004) conclude that the asymmetry is caused by the remnant encountering the ancient nebula in the South-West region and therefore the optical remnant in that particular part should be slowed down compared to the rest of the remnant. To find out if the deceleration has occurred in the South-West region was the main reason to measure proper motions of the individual knots.

2.2 Optical imaging: time series

We used 19 images of GK Persei, obtained between the years 2004–2011, for measuring the movement on the plane of the sky and the flux-variability of the knots. Most of the imaging was done with 2.54 m Isaac Newton Telescope (INT), using the Wide Field Camera (WFC). Images were also obtained with the Nordic Optical Telescope, with ALFOSC UV-optical imaging camera[3]. We also used five archival images of Nova Persei, taken with INT with Prime Focus Cone Unit (PFCU), Hubble Space Telescope with Wide-Field Planetary Camera 2 (WFPC2) and Palomar 48 inch Samuel Oschin Telescope (P48). An overview of the optical imaging observations are given in Table 1 in chronological order, with the observation date in the first column, used telescope and instrument in the second and filter with central wavelength and bandpass in the third column.

All frames were already bias, flat field corrected and matched pixel-by-pixel to the reference frame, the 2004 INT image. Matching was needed to simplify the measurements in pixel coordinate system. For brightness measurements, most of the INT+WFC images were flux matched, again using the 2004-01-29 INT image as a reference. The scope of the current work with the images was to contribute in the measurements, not in data reduction. See Liimets et al. (2012) for more information about the data reduction.

[3]The data presented here were obtained [in part] with ALFOSC, which is provided by the Instituto de Astrofisica de Andalucia (IAA) under a joint agreement with the University of Copenhagen and NOTSA.

Table 1: Optical images used for measuring the proper motion. The images used for measuring fluxes are marked with a superscript ^{f}. Images from archive are marked with an asterix *. The reference image is in bold.

Date	Telescope + instrument	Filter (λ_{cent}/bandpass (Å))
1987-07-27*	INT+PFCU	R (6460/1290)
1989-10-05*	P48	photographic plate
1995-11-08*	HST+WFPC2	F658N [NII] (6590/22)
1997-01-08*	HST+WFPC2	F658N [NII] (6590/22)
1999-11-30*	INT+WFC	Hα (6568/95)
2004-01-29^f	INT+WFC	Hα (6568/95)
2004-08-04^f	INT+WFC	Hα (6568/95)
2004-09-03^f	INT+WFC	Hα (6568/95)
2004-12-30^f	INT+WFC	Hα (6568/95)
2005-09-16^f	INT+WFC	Hα (6568/95)
2006-10-12^f	INT+WFC	Hα (6568/95)
2007-01-04^f	INT+WFC	Hα (6568/95)
2007-03-01^f	INT+WFC	Hα (6568/95)
2007-09-03	NOT+ALFOSC	Hα (6577/180)
2007-09-05	NOT+ALFOSC	Hα (6577/180)
2007-09-07^f	INT+WFC	Hα (6568/95)
2008-01-08^f	INT+WFC	Hα (6568/95)
2008-08-19^f	INT+WFC	Hα (6568/95)
2008-09-12	INT+WFC	Hα (6568/95)
2008-11-14^f	INT+WFC	Hα (6568/95)
2009-02-11	NOT+ALFOSC	Hα (6577/180)
2009-12-08	INT+WFC	Hα (6568/95)
2010-02-09^f	INT+WFC	Hα (6568/95)
2011-12-13^f	INT+WFC	Hα (6568/95)

3 Spectroscopy of the nova remnant Nova Persei 1901

3.1 Spectrum of a nova remnant

Radiation from a star is a good approximation of black body radiation, which gives a continuous spectrum. However, when dispersing the radiation from a star, dark absorption lines are revealed. Absorption lines are produced when cooler gas in the star's atmosphere absorbs photons with certain wavelength, so atoms or ions go to an excited state (Emerson 1997, p. 41-42). These are known as Fraunhofer lines, named after physicist Joseph von Fraunhofer, who in 1814 catalogued the lines in the solar spectrum (Moore & Rees 2011, p. 10-11). The spectrum of the matter expelled from a star is, on the other hand, an emission spectrum. The emission lines are produced in de-excitation of atoms and ions when they have previously been excited in recombination and collisional processes and which results in emitting photons of certain wavelength. In this type of nebula, ions are more common than neutral atoms, due to the photoionization of atoms with ultraviolet photons originated from the central star and/or shock ionization (Emerson 1997, p. 187; Osterbrock & Ferland 2006, p. 316).

Recombination lines are produced when an atom, a product of recombination of an ion and an electron, goes from an excited state to more stable lower-energy states by emitting photons. Process continues until the lowest energy state is reached. Due to the low density of the nebula, the number of recombinations is low, so the recombination lines of only abundant elements are usually detected. Collisions between elements (or usually ions and electrons) also produce emission lines. Collisions can excite the atom or ion. This depends on kinetic energies of the colliding particles and the excitation energies of the atoms or ions: the kinetic energies should be in the same order than the excitation energy. Ions have energy levels farther apart than atoms, so higher kinetic energies (temperatures) are needed for this process. Collisions can also de-excite atoms and ions, but the released energy is carried away by the colliding electron, so no radiation is emitted. In an optically thin environment, like in a gaseous nebula, "forbidden" emission lines are produced. If an atom or an ion is in an excited state (due to collision), a radiative transition from or between meta-stable energy levels may occur. In low density conditions, collisional de-excitations are rare, so forbidden lines can be seen. Even in vacuums made in laboratories, the atoms will be always collisionally de-excited before there is time for a forbidden radiative decay (Emerson 1997, p. 189-192). The main part of emission lines in the optical region are collisionally excited forbidden lines (Osterbrock &

Ferland 2006, p. 67).

The spectrum holds information about the chemical and physical conditions inside the remnant. Nova shell is a mixture of gas from both stars in the system – hydrogen and helium from outer layers of the subgiant and heavier elements from the white dwarf (Osterbrock & Ferland 2006, p. 295-296). Inside the gaseous filaments of the remnant, collisions between electrons and electrons and ions distribute energy. The source of the energy can be ultraviolet radiation from the central star, when the star's effective surface temperature is more than 3000 K. Photons are absorbed and photoelectrons released; the excess energy of the photon transforms into the kinetic energy of the electron. Nova remnants can also be shock-heated, due to the high velocity of the ejecta running into the interstellar medium. Another possibility is that there is no source of new energy. Regardless of the source for the energy, the gas has a Maxwell-Boltzmann velocity distribution with electron temperature T (Osterbrock & Ferland 2006, p. 7-8,11-12). Our motivation for investigating the spectrum of nova remnant Nova Persei 1901 was to find out the electron temperatures inside the gas-clumps.

3.2 Long-slit spectroscopy

For determining electron temperature inside the gaseous filaments of the remnant, long-slit spectroscopy was used. Long-slit spectrum gives spectral and spatial information for an object, although only in one direction. Thus, we get many spectra over the chosen spatial direction.

The long-slit spectrum of GK Persei (Figure 2) was taken with the 2.56 m Nordic Optical Telescope using The Andalucia Faint Object Spectrograph and Camera (ALFOSC) in 6th September 2007 with exposure time of 1200 seconds. ALFOSC can be used for spectroscopy, as well as for photometry. The position angle of the slit, measured from north eastwards, was 111 degrees (as shown on Figure 3). The long-slit that was used covers the full spatial field of view of the instrument (6.3 arcminutes), with a width of 0.5 arcseconds. The dispersing elements in ALFOSC are combinations of prisms and a diffraction gratings – grisms. Low resolution grism #4 was used, with a central wavelength of 5800 Å and a wavelength diapason of 3200-9100 Å, which corresponds to the optical waveband. Correction (bias and flat-field) and calibration (lamp and standard star spectra) exposures were done on the same observation night. Spectrum of spectrophotometric standard star BD+332642 had a 60 second and standard star BD+254655 30 second exposure time, done with the same instrument mode, using grism #4.

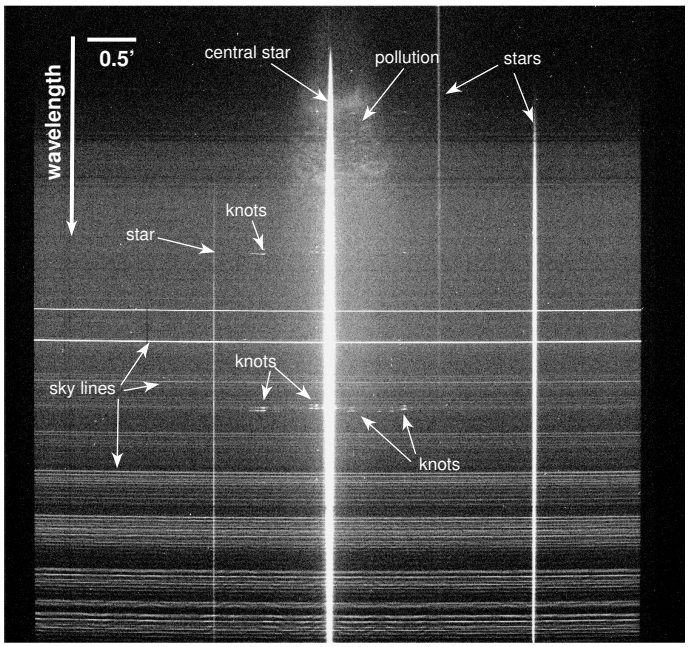

Figure 2: Raw long-slit spectrum of GK Persei (NOT+ALFOSC, 2007-09-06). Wavelength axis: up to down corresponds to blue to red; spatial axis is horizontal. Thick vertical line is the overexposed central star, fainter lines, parallel to the central star, are other stars accidentally placed on the slit. Horizontal lines are the night sky emission lines, small bright speckles are the cosmic rays. On the upper part of the spectrum, close to central star, a scattered light pollution is visible. Knots are brighter, larger spots closer to the central star

ALFOSC is used for low and medium resolution spectra. Spectral resolution $\delta\lambda$ shows how close can two spectral lines be, to be still detected as separate lines. Resolving power is the ratio

$$R = \frac{\lambda}{\delta\lambda} \ . \tag{1}$$

This ratio describes the spectrograph, but is also dependent on the brightness of the object and the quality of the telescope (Chromey 2010, p. 92).

The resolution was measured on the calibration lamp spectrum on five different helium lines. Lamp spectrum is a long-slit spectrum taken of a helium lamp, therefore the spectrum consists of He emission lines only. Lamp spectrum does not suffer as much from line broadening, it is only dependent on the instrument. The dispersion of grism #4 is 3.0 Å/px, the average full width at half maximum (FWHM) of a Gaussian fitted He line is 2.5 px, so the resolution is 7.5 Å. In the blue part of the spectrum on Figure 2, the resolving power is 518 (measured at $\lambda = 3888$ Å), in the middle 667 ($\lambda = 5015$ Å) and in the red end of the spectrum it is 970 (λ7281 Å).

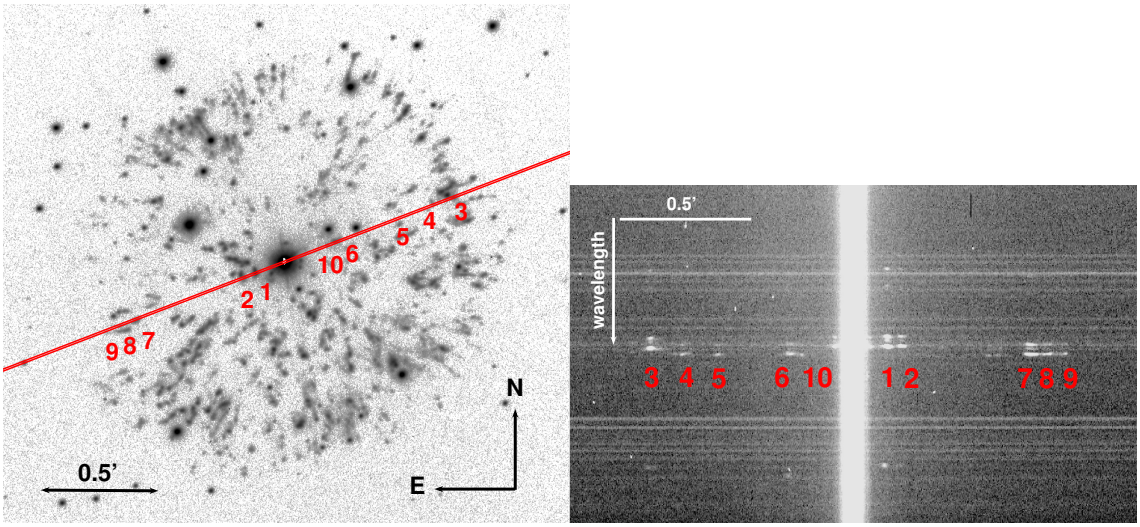

(a) slit (b)

Figure 3: a) GK Persei narrowband $H\alpha$ image (NOT+ALFOSC 2007-09-04). The red line shows the slit's position on top of the nova remnant b) Brightest emission lines of ten knots on the two-dimensional long-slit spectrum of GK Persei. The wavelength axis is from top to bottom.

3.3 Reduction of the long-slit spectrum

Raw data must be first reduced (bias and flat-field corrected) to eliminate instrumental artefacts. The spectrum should also be wavelength and flux calibrated to go from instrumental to physical units. For this we used the Image Reduction and Analysis Facility (IRAF[4] for short) and followed a standard reduction process: bias subtraction, flat-field correction, wavelength calibration, removal of sky lines and flux calibration.

During the observation night, zero-exposure (bias) images were obtained, taken without opening the shutter. Although, with zero exposure time the CCD pixels should have zero values, they still have positive values due to electronic offset (to ensure that the Analogue-to-Digital Converter will always receive a positive signal). This bias level should be subtracted from the science frame and also from the flat field and standard star frames. We corrected the bias level with the overscan region (the "empty" regions on the edges of the frame on Figure 2) and with the bias frames using tasks *zerocombine* and *ccdproc* in the IRAF/NOAO/IMRED/CCDRED package. When overscan processing subtracts the mean zero level, bias frame itself corrects for the pixel-to-pixel bias differences all over the frame. For no double-subtraction, overscan correction was done also for the so called master-bias

[4] IRAF is distributed by the National Optical Astronomy Observatory, which is operated by the Association of Universities for Research in Astronomy (AURA) under cooperative agreement with the National Science Foundation.

frame (a bias frame, which consists of averaged zero level pixel values from all acquired bias frames) (Chromey 2010, p. 288-290).

Some parts of the science frame (and in the same manner other reduction and calibration frames) were trimmed out in order to only have a scientifically useful area of the two-dimensional spectrum: the central star together with the emission from the knots of the nova remnant.

Twilight and lamp flat-field exposures were used for correcting pixel-to-pixel differences which arise from variations in detector's sensitivity, heterogeneous illumination due to optical system and effects of dust and scratches (Chromey 2010, p. 292-293). Because of the grism used, from the wavelength of 6700 Å a fringing pattern occurs, getting worse in the red wavelengths (peak-to-peak fringe levels 20-25%, when >8000 Å[5]). Fringing pattern is a brightness pattern caused by reflection and interference within the thin layers of the CCD due to night sky emission lines, this can also be reduced by flat-field correction (Chromey 2010, p. 297). Lamp flat-field frames were taken of the internal halogen lamp and were used for correcting the pixel-to-pixel variations; twilight sky flat frames were used for correcting illumination differences of the spectrum of GK Persei. Also, spectra of standard stars and the comparison spectrum were flat field corrected. Flat field reduction was made using tasks *flatcombine* and *ccdproc* in the package mentioned before, also *response* and *illumination* from NOAO/TWODSPEC/LONGSLIT package were used. As seen from Figure 4, the wavy pattern in the red end of the spectrum could not be fully eliminated with flat-fielding, although it was reduced. Fringing is caused by the night sky emission lines, which change throughout the observing night; the task removing them fully is known to be difficult (Massey 1997, p. 2-4).

After data correction, the science frame was calibrated for wavelength and flux. Helium lamp was used as a comparison spectrum for wavelength calibration. We used an Helium arc lamp map provided for wavelength band of grism #4 by NOT[6] to find and define the right emission lines on the comparison spectrum and carried wavelengths over to the science and standard star frames. This was done using tasks *identify*, *reidentify* and *transform* in the LONGSLIT package. As a result, we got wavelength in angstroms instead of original units pixels. For converting analog-to-digital units (ADU) to flux units (erg$\cdot$ s$^{-1}\cdot$ cm^{-2}), we used spectra of two spectrophotometric standard stars (BD+332642 and BD+254655, see Appendix 10.1). The long-slit spectra of standard stars were reduced, as described before, and one-

[5]Information on ALFOSC grisms: `http://www.not.iac.es/instruments/alfosc/grisms/`
[6]ALFOSC arc lamp maps: `http://www.not.iac.es/instruments/alfosc/lamps/`

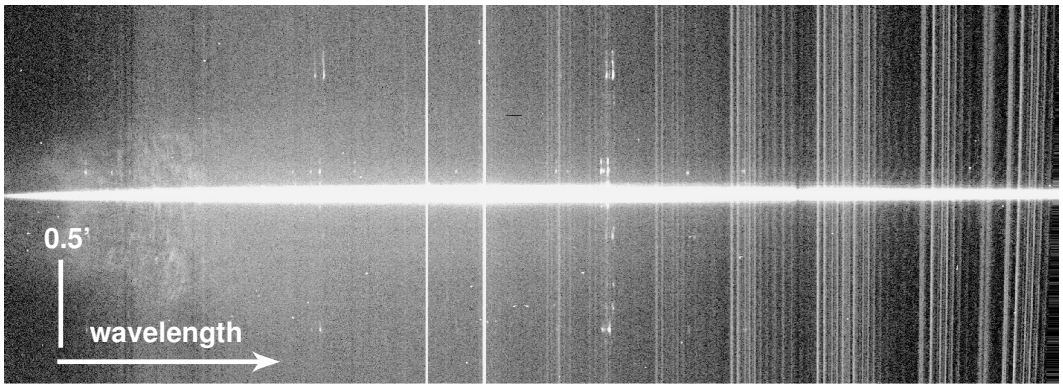

Figure 4: Bias and flat-field corrected and trimmed two-dimensional long-slit spectrum of GK Persei. Note that this image is turned 90 degrees to the left and uses a different gray-scale display, compared to Figure 2.

dimensional spectra were extracted. The energy distributions of standard stars are known and so the flux-calibrated spectrum of the object in interest can be derived. The flux-calibration was done using IRAF tasks *sensfunc* in ONEDSPEC and *calibrate* in TWOSPEC/LONGSLIT package.

For precise flux calibration and measurement, we carefully determined knots' apertures in spatial direction and extracted them from the two-dimensional long-slit spectrum of Nova Persei, using the IRAF task *apall*. This was done between wavelength and flux calibration. Also, night-sky emission lines, what are caused by different processes in the Earth's upper atmosphere, were eliminated at this phase. One-dimensional emission spectrum was extracted for ten knots (knot-1 shown on Figure 3, knot-2 and knot-3 in Appendix 10.2). The blue end of the spectrum was polluted with scattered light in the instrument (see Figure 2 and 4). This was inhomogeneous in nature, so even with careful background subtraction and taking into account the sensitivity of the CCD for different wavelengths, the effects could not be totally removed.

4 Measurements and analysis

4.1 Imaging: proper motions of the individual knots

The apparent expansion of the remnant of GK Persei in the plane of the sky, resolvable even in monthly time intervals with ground based telescopes, gives a good opportunity to study the evolution of the matter outflow. Because the ejected matter is in clumps ("knots"), proper motions of these were measured when the individual knots were resolvable in most of the 19 main images. The pixel scale (0.33 arcsec/px for INT images, 0.19 arcsec/px for NOT) and quality of our images enabled us to resolve and measure 283 knots out of which the author of the current bachelor thesis measured 110 (see Figure 5). As mentioned before, archival images were also provided (see Table 1) – they were with poorer quality and were measured if the knot under inspection was resolvable. The purpose of these images was to detect any accelerations or decelerations in the past and also to support the analysis of the main data.

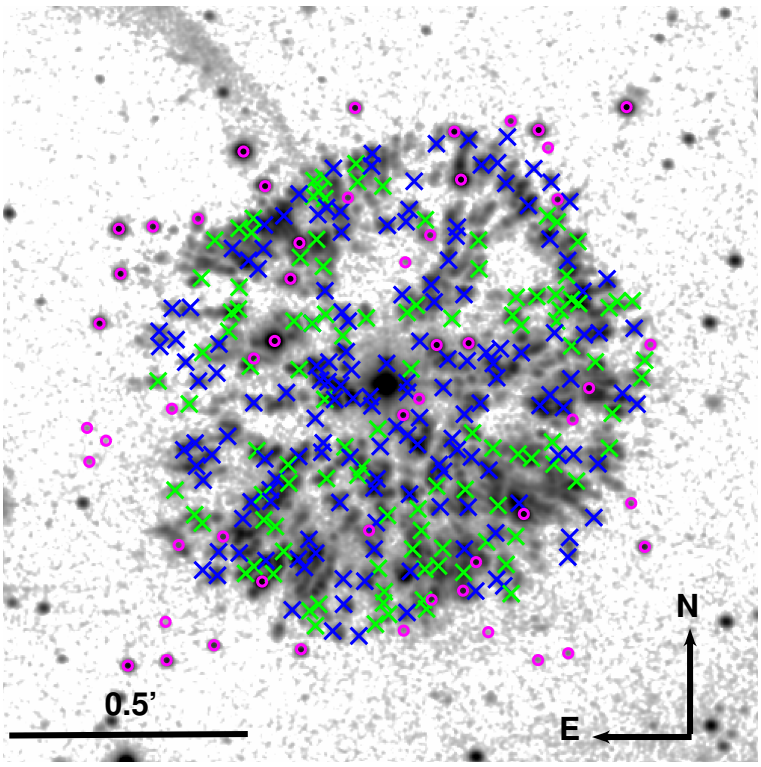

Figure 5: Example Hα image that was used in measurements (INT+WFC 2010-02-09). Knots with measured proper motions are marked with x: knots measured by the author are marked with green; knots measured by others with blue; pink circles are background stars.

For measuring the movement of the knots on the plane of the sky, we first visually identified a knot on all images. Because of almost isotropic expansion of the remnant, a knot was easily found on other frames, when we identified it on a reference image. Problems arose when the knots were a close-set, blurred together with a neighbouring knot or with a bigger clump of knots. In some cases, a knot was isolated on later images, but was merged with another knot on earlier frames or *vice versa*.

Most of the knots are round, so we used apertures for the measurements. The diameter of a knot was determined visually according to the size of the knot on a reference frame, adding two pixels for background fit. We used IRAF task *imexamine* to measure the central coordinates of the knots on each frame using the Gaussian fit in X and Y direction inside the aperture and assessed fitting parameters individually. A program created for the measurements aided the process by providing input frames to the IRAF task in the right chronological sequence one after another. Output file was a list with the names of the measured frames and corresponding central coordinates (in pixel-units) in X and Y direction.

4.2 Imaging: brightness evolution

Apparent brightness is the total energy per unit time per unit area that arrives from the source. This measure is also called flux or flux density; in physics this measure is known as irradiance (all wavelengths) or illuminance (visual light) (Chromey 2010, p. 13-14). In our case, most of the frames were taken with the same telescope and instrument. 14 INT frames were flux-matched to study the brightness evolution of the cirumstellar matter (see Table 1) by measuring the relative brightnesses, as the used images were not flux calibrated. This means that the measurements were done in original, but normalised (to 2004-01-29 image) analog-to-digital units (ADU), not in physical units described above.

Fluxes were measured in the IRAF environment, using a script made for the task. The script was based on knot's coordinates measured when proper motions were determined. Also, the same apertures were used. The background (sky) flux was taken from the sky annulus, which started 3 pixels distance from the knot's aperture and had a width of 4 pixels (example shown on Figure 6b). As a result, integrated flux in the corresponding aperture was measured, frame-by-frame and knot-by-knot. The real flux of the knot was calculated:

$$flux = sum - area \cdot msky, \tag{2}$$

where *sum* is the total flux measured in the knot's aperture, *area* is the area of the sky annulus in square-pixels and *msky* is the best estimate of the sky value per pixel (eliminating the high flux pixels). We measured flux evolution of 190 knots (marked with green x-es on Figure 6a).

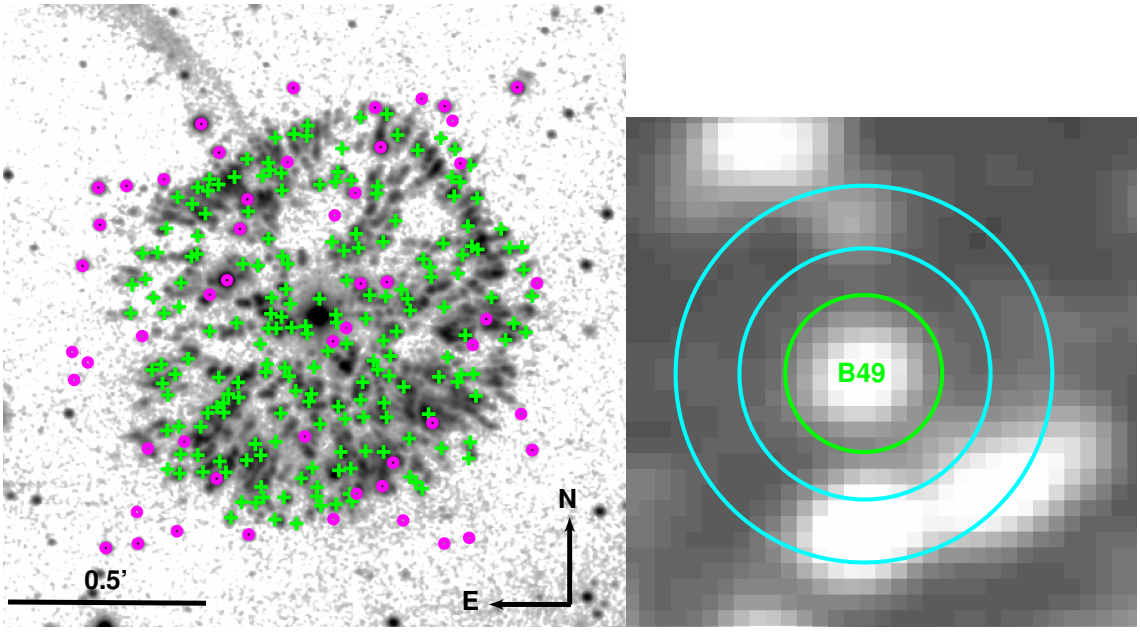

(a) (b)

Figure 6: Example Hα image that was used in flux measurements (INT+WFC 2010-02-09). a) Knots with measured flux are marked with a green cross; pink circles are background stars. b) Example of a close up of a knot B49: knot's aperture is the green circle, sky annulus is marked with cyan.

4.3 Spectroscopy: emission line flux

The emission spectrum holds information about physical characteristics of a nebula. The spectrum depends upon the abundances of the elements, which in turn is dependent on the ionization, temperature, density and the history of the nebula (Osterbrock & Ferland 2006, p. 67-68). We used IRAF task *splot* to measure integrated fluxes of the Gaussian fitted spectral lines relative to defined background level on the one-dimensional spectra. This method made the measurements in the blue end of the spectrum, where the background is above zero, relatively correct. 14 spectral lines were resolvable in the spectrum of the brightest knot-1 (Figure 7 and Table 2), less on the others. After measuring, we identified the spectral lines by comparing measured wavelengths to laboratorial wavelengths. We also checked for cosmic rays, which are very high-energetic particles that bombard Earth (and used CCD). On our long slit spectrum, they appear as "spikes", affecting only one or two pixels. On the one-dimensional spectra, they can be confused with a real spectral

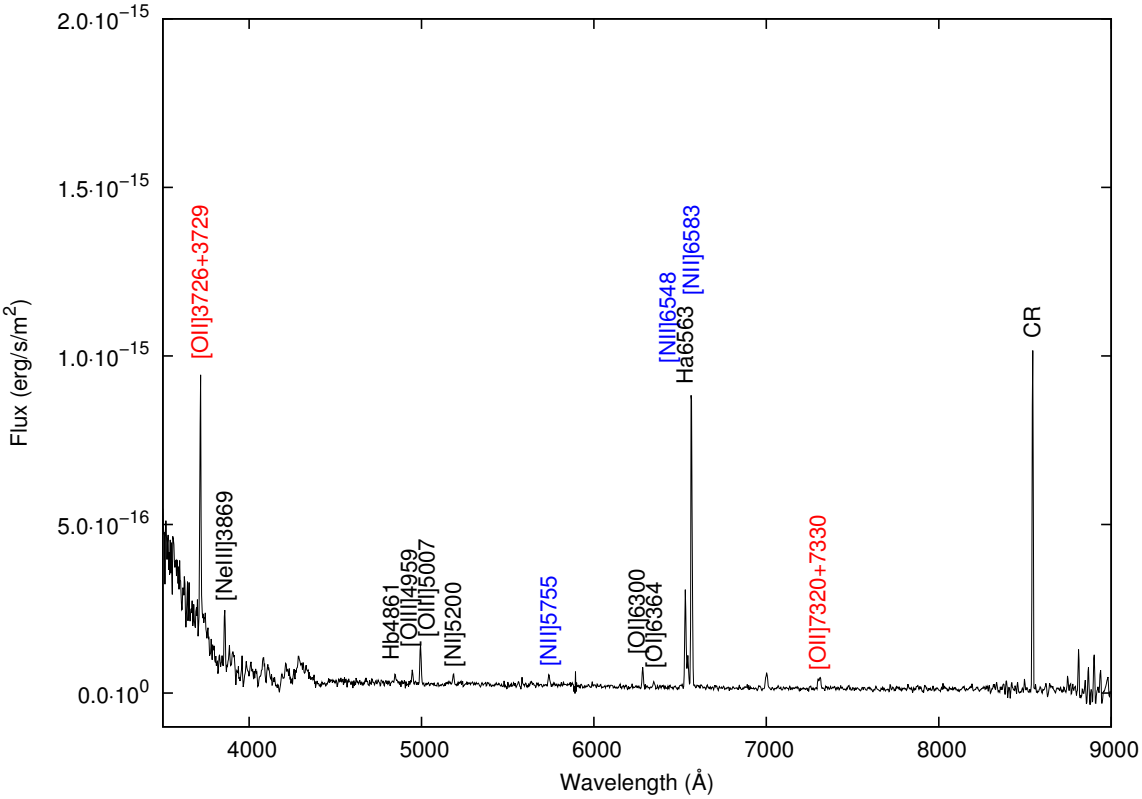

Figure 7: One-dimensional spectrum of the brightest knot with identified lines. A cosmic ray (CR) line is visible on 8500Å, problematic background flux in the blue and fringing pattern in the red wavelengths. Emission lines used in temperature estimation are marked with red ([OII]) and blue ([NII]).

line, like seen from Figure 7. Ordinarily, cosmic rays should be removed during reduction process, but we could not risk mistaking a cosmic ray and an emission line. On a one-dimensional spectrum, emission lines can be identified, cosmic rays are usually abnormally bright and with a random placement.

Interstellar dust between the observer and the object leads to absorption and scattering – extinction – of electromagnetic light coming from the object. This is dependent on wavelength, as shorter (bluer) wavelengths are more easily absorbed and scattered by dust, hence a star looks more red than it really is (reddening). All emission line fluxes need to be compensated for the extinction. This can be done using the extinction law:

$$I = I_0 \cdot 10^{-C_\beta \cdot f(\lambda)} \ , \tag{3}$$

where I_0 is the corrected flux, I is the measured flux, f(λ) is the normalized extinction function and C_β is the logarithmic extinction at Hβ-line (f(Hβ)=1) (Corradi 2014). C_β depends on the star, but the function f(λ) is the same for most stars in the

Galaxy and these extinction curves can be found in different forms from the literature (Osterbrock & Ferland 2006, p. 177-179). We used the extinction curve from a study by Fitzpatrick & Massa (2009), where they provide

$$a(\lambda) = \frac{E(\lambda - V)}{E(B - V)} = \frac{A(\lambda) - A(V)}{A(B) - A(V)} \ , \tag{4}$$

where $A(\lambda)$ is extinction in a certain wavelength and $A(V)$ and $A(B)$ are extinctions in visual V and B wavelengths. They have determined the shape of the extinction curves from ultraviolet to infrared wavelengths by modelling the spectral energy distributions of reddened early-type stars, that fit well with stellar atmosphere models. The curves vary for different total to selective extinction ratios R_V, which is a quantity that can be calculated for every object based on observational information (Mathis 1990):

$$R_V = \frac{A(V)}{E(B - V)} \ . \tag{5}$$

We used the value $R_V = 3.0$ which was calculated using values for GK Per from literature: $A_V = 0.96$ mag (Wu et al. 1989) and E(B-V)= 0.32 mag (Shara et al. 2012) and which is close to the standard value within the Galaxy, 3.1 (Osterbrock & Ferland 2006, p. 179).

The relation between f(λ) in equation 3 and the a(λ) provided by Fitzpatrick & Massa (2009), was found using the relation

$$C_\beta \cdot f(\lambda) = 0.4 \cdot A_\lambda = 0.4 \cdot A_V \cdot \frac{A_\lambda}{A_V} = 0.4 \cdot A_V \cdot (1 + \frac{a(\lambda)}{R_V}) \ . \tag{6}$$

For Hβ(4861) line at 4848 Å: a(4848)=0.5381809 and f(4848)=1, so

$$A_V = 2.1197 \cdot C_\beta \ , \tag{7}$$

$$f(\lambda) = 0.84789 \cdot (1 + \frac{a(\lambda)}{R_V}) \ . \tag{8}$$

C_β depends on the star and is calculated usually using Hα and Hβ flux ratio, considering normalization, equation 3 and a(6545)=-0.75908775 for Hα line:

$$C_\beta = 2.7274 \cdot log(\frac{\frac{H\alpha}{H\beta}}{\frac{H\alpha_0}{H\beta_0}}) \ , \tag{9}$$

where Hα and Hβ are the observed fluxes of corresponding lines and Hα_0 and Hβ_0 are the intrinsic values (that can be acquired from literature) (Corradi 2014). In our spectra, hydrogen lines give a ratio 3.77 and the intrinsic intensity ratio for our case (assuming nebula is optically thick to ionizing radiation ("Case B" nebula) and

T=$2 \cdot 10^4$ K) is 2.76 (Osterbrock & Ferland 2006, p. 68-73), so $C_\beta = 0.369$. A python script (see Appendix 10.3) was written by the author of current Bachelor's thesis to aid the calculations. Extinction due to atmosphere has similar effect, but this was corrected simultaneously with flux calibration.

By obtaining the fluxes of certain emission lines, physical properties electron temperature and electron density can be calculated. These two properties are tied together, so one can be calculated assuming the other. This method is usable when the density of the environment is low, which is the case with Nova Persei's remnant. The temperature in a nebula can be determined by using ratios of intensities of pairs of emission lines that are emitted by a single ion from two levels with substantially different excitation energies (Osterbrock & Ferland 2006, p. 107-119). In our spectra, the suitable pairs are [OII] 3726+3729 and 7320+7330 (Å) and [NII] 6548+6583 and 5755 (Å) emission lines (marked with colors in Figure 7).

For the emission line diagnostics, we used a task *temden* in IRAF/STSDAS/ANALYSIS/NEBULAR, developed by De Robertis et al. (1987) and made into a IRAF package by Shaw & Dufour (1995). The task uses the ratios of certain (extinction-corrected) emission lines of a certain ion and the assumed electron density of the nebula. The ratio $\frac{j(3726+3729)}{j(7320+7330)}$ was used for [OII], and $\frac{j(6548+6583)}{j(5755)}$ for [NII], where $j(\lambda)$ marks the redden-corrected intensity of an emission line. Knot-1 has enough lines to do emission line diagnostics with both [NII] and [OII] lines, knot-2 and knot-3 have needed emission lines for the oxygen ion. From ten extracted spectra, three were usable for temperature measurements. Shara et al. (2012) measured electron densities (assuming temperatures) with a similar method from two of the brightest knots in the study and got $(3.5 \pm 2.0) \cdot 10^3$ cm^{-3}. Due to absence of [SII] 6717 and 6731 (Å) lines and the blend of [OII] 3726 and 3729 (Å) lines, the density estimation is not possible with our data (Osterbrock & Ferland 2006, p. 121-127). We assumed a variety of electron densities inside a knot, from (0.5–5.5)$\cdot 10^3$ cm^{-3}.

Temperature estimation with this method is sensitive to flux calibration and reddening correction of emission lines, uncertainties are large and their estimation problematic. The noisy blue part of the spectrum affects the flux of [OII]3728 doublet. Also, fringing in the red part may affect the [OII]7325 doublet in the red. The latter could also be affected by recombination effect. Uncertainties in the flux calibration and reddening correction also affect the [OII] diagnostic due to the large wavelength separation of the two [OII] doublets. Because the [NII] lines are less affected by these effects, temperature estimation using [NII] should be considered significantly more reliable. We assume flux calibration and reddening correction is good in a 10% error

margin for [NII] and 30% for [OII] emission line flux measurements. These errors were carried over to temperature calculations and the combining error is dependent on the ratios of emission lines with errors, the density and the theoretical possibility for such emission line ratios.

5 Results

5.1 Results for the optical imaging time series

The aim of the current work with the images was to contribute to the measuring process. The proper motion and flux measurements gave scientifically valuable data for the study of the evolution of stellar outflow of GK Persei and the results are published in Liimets et al. (2012), where velocities, kinematical ages, decelerations/accelerations, flux evolution and the apparent expansion of the nebula were found. The expansion of the nebula of GK Persei is well sampled during the 7 years of observations (25 years, with archival images). The knots' two dimensional velocities also got also a third dimension, radial velocity from spectroscopic observations, so making it *A Three-dimensional View of the Remnant of Nova Persei 1901 (GK Per)*. The data from archival images accompanied the main data and helped to detect any accelerations and decelerations during the longer time interval. The results published in Liimets et al. (2012) were interesting: contrary to studies published before (e.g Bode et al. (2004)), we found no evidence of uneven expansion in different directions of the remnant, even in the South-West quadrant. Proper motion measurements combined with radial velocity measurements from spectroscopic data showed that the velocities of knots in the nova remnant's shell range from 250 to 1100 km/s (with majority in the 600 and 1000 km/s range). Kinematical ages, which are indicators of decelerations/accelerations of knots, were also calculated using results from proper motion measurements. These ages range from 96 to 170 years, with a mean value of 118 years. At the time of the publication, 103 years had passed from the nova explosion, hence there has been a slight deceleration of the nova shell.

The brightness evolution measurements of individual knots showed surprisingly varying results when compared to the brightness decline of the whole remnant, which was also measured during the study of Nova Persei 1901. The total Hα+[NII] flux of the nebula has been linearly decreasing at a rate of 2.6% per year. Out of the 190 knots measured for current Bachelor's thesis, 85 were used in data analysis for Liimets et al. (2012). From these, 50% show similar consistent fading (example shown on Figure 8a), 15% of knots have constant flux, 20% show brightening and 15% have fast fading or brightening (or both) (example shown on Figure 8b).

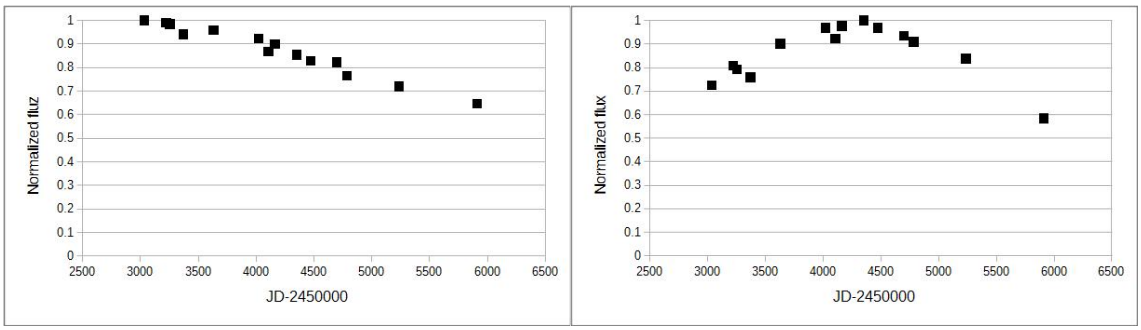

(a) (b)

Figure 8: Illustrative example of flux evolution of a knot with a) consistent fading, b) brightening and fading. Time-axis is in Julian date (JD)[7], the flux is normalised to the maximum flux of a knot.

5.2 Emission lines in the optical spectrum

As seen from Table 2, 14 emission lines are revealed in the optical spectrum of the brightest knot. This spectrum is typical for an ionized nebula such as HII regions, planetary nebulae, or other ionized stellar outflows. Most of the emission lines are forbidden lines, symbolized by square brackets. Only the Balmer Hα and Hβ emission lines are recombination lines. As described in Section 3, recombinational emission lines are produced only with abundant elements and hydrogen is the most abundant element in the nebula. Helium is the second most abundant element in the nebula. No He lines are seen in the spectrum, likely because they are below the detection limit of the present observations. Typical nebular emission lines such as [NII], [OIII] and [OII] dominate the spectrum. The emissivity of these forbidden lines strongly depends on electron temperature and density and so, as also done in this thesis, can be used to determine the electron temperature in the remnant. Perhaps surprisingly, we do not observe the [SII]6717, 6731 (Å) doublet which is a standard density indicator, and is usually enhanced in shock-excited gas (Osterbrock & Ferland 2006, p. 303).

[7]Julian date is a number of (UT) days elapsed since 4713 BC, January 1, 12:00 (Chromey 2010, p. 87).

Table 2: Identification and measurements of emission lines from one-dimensional spectra of knot-1, knot-2 and knot-3. First column shows the emission line and it's laboratory wavelength, second column the measured wavelength, third and fourth column show measured flux and redden-corrected flux accordingly.

Knot-1			
Spectral line & λ_{lab} (Å)	Measured λ (Å)	Flux (erg/(s· cm^2))	Flux$_{corr}$ (erg/(s· cm^2))
$[OII]$ 3726+3729	3717.994	$5.915 \cdot 10^{-15}$	$1.792 \cdot 10^{-14}$
$[NeIII]$ 3869	3858.556	$1.239 \cdot 10^{-15}$	$3.638 \cdot 10^{-15}$
$H\beta$ 4861	4847.566	$2.427 \cdot 10^{-16}$	$5.656 \cdot 10^{-16}$
$[OIII]$ 4959	4946.864	$3.429 \cdot 10^{-16}$	$7.812 \cdot 10^{-16}$
$[OIII]$ 5007	4994.255	$1.125 \cdot 10^{-15}$	$2.536 \cdot 10^{-15}$
$[NI]$ 5200	5185.116	$2.807 \cdot 10^{-16}$	$6.070 \cdot 10^{-16}$
$[NII]$ 5755	5739.274	$3.374 \cdot 10^{-16}$	$6.550 \cdot 10^{-16}$
$[OI]$ 6300	6282.838	$5.221 \cdot 10^{-16}$	$9.281 \cdot 10^{-16}$
$[OI]$ 6364	6347.453	$1.691 \cdot 10^{-16}$	$2.978 \cdot 10^{-16}$
$[NII]$ 6548	6530.377	$2.721 \cdot 10^{-15}$	$4.670 \cdot 10^{-15}$
$H\alpha$ 6563	6544.578	$9.152 \cdot 10^{-16}$	$1.568 \cdot 10^{-15}$
$[NII]$ 6583	6565.587	$8.283 \cdot 10^{-15}$	$1.415 \cdot 10^{-14}$
$[OII]$ 7320	7300.051	$1.934 \cdot 10^{-16}$	$3.026 \cdot 10^{-16}$
$[OII]$ 7330	7311.277	$4.092 \cdot 10^{-16}$	$6.395 \cdot 10^{-16}$
Knot-2			
$[OII]$ 3726+3729	3717.527	$1.279 \cdot 10^{-15}$	$3.874 \cdot 10^{-15}$
$[OIII]$ 5007	4994.695	$2.902 \cdot 10^{-16}$	$6.540 \cdot 10^{-16}$
$[NII]$ 6548	6530.389	$6.050 \cdot 10^{-16}$	$1.038 \cdot 10^{-15}$
$H\alpha$ 6563	6545.27	$1.282 \cdot 10^{-16}$	$2.196 \cdot 10^{-16}$
$[NII]$ 6583	6565.583	$2.001 \cdot 10^{-15}$	$3.417 \cdot 10^{-15}$
$[OII]$ 7320	7300.02	$5.313 \cdot 10^{-17}$	$8.313 \cdot 10^{-17}$
$[OII]$ 7330	7311.241	$1.624 \cdot 10^{-16}$	$2.538 \cdot 10^{-16}$
Knot-3			
$[OII]$ 3726+3729	3722.192	$2.178 \cdot 10^{-15}$	$6.591 \cdot 10^{-15}$
$[NeIII]$ 3869	3862.477	$8.857 \cdot 10^{-16}$	$2.599 \cdot 10^{-15}$
$[OIII]$ 4959	4952.092	$2.076 \cdot 10^{-16}$	$4.724 \cdot 10^{-16}$
$[OIII]$ 5007	4998.932	$7.900 \cdot 10^{-16}$	$1.779 \cdot 10^{-15}$
$[NII]$ 6548	6537.241	$8.046 \cdot 10^{-16}$	$1.380 \cdot 10^{-15}$
$H\alpha$ 6563	6550.624	$3.507 \cdot 10^{-16}$	$6.002 \cdot 10^{-16}$
$[NII]$ 6583	6572.878	$2.730 \cdot 10^{-15}$	$4.658 \cdot 10^{-15}$
$[OII]$ 7320	7306.063	$6.009 \cdot 10^{-17}$	$9.396 \cdot 10^{-16}$
$[OII]$ 7330	7320.135	$1.680 \cdot 10^{-16}$	$2.623 \cdot 10^{-16}$

5.3 Electron temperature inside the gaseous clumps

The results for emission line diagnostics for three knots with the required emission lines are presented in Table 3. As predicted in Section 4.3, the [OII] results are more sensitive to density change – the decrease in temperature with increase of density is rapid. Some ratios of [OII] emission line fluxes are theoretically impossible for temperature assessment, so the task *temden* task could not give numerical values in some cases: at lower densities, some of the values and error estimations are missing. The errors are then substituted with the higher density's temperature error, although the error should be larger. It is coincidental that in lower densities

Table 3: Calculated electron temperatures in knots 1, 2 and 3 for assumed electron densities, using [NII] and [OII] emission line diagnostics

		Knot-1	Knot-2	Knot-3
assumed density (cm^{-3})	element [NII]/[OII]	calculated T 10^4 (K)	calculated T 10^4 (K)	calculated T 10^4 (K)
500	[NII]	$1.99(^{+0.25}_{-0.18})$	–	–
1000	[NII]	$1.97(^{+0.20}_{-0.22})$	–	–
1500	[NII]	$1.95\ (^{+0.22}_{-0.19})$	–	–
2000	[NII]	$1.93\ (^{+0.22}_{-0.19})$	–	–
2500	[NII]	$1.91\ (^{+0.21}_{-0.19})$	–	–
3000	[NII]	$1.88\ (^{+0.21}_{-0.18})$	–	–
3500	[NII]	$1.86\ (^{+0.23}_{-0.16})$	–	–
4000	[NII]	$1.84\ (^{+0.22}_{-0.16})$	–	–
4500	[NII]	$1.82\ (^{+0.22}_{-0.16})$	–	–
5000	[NII]	$1.81\ (^{+0.21}_{-0.15})$	–	–
5500	[NII]	$1.79\ (^{+0.21}_{-0.15})$	–	–
500	[OII]	$1.59\ (^{+0.72}_{-0.36})$	–	$1.63\ (^{+0.55}_{-0.38})$
1000	[OII]	$1.27\ (^{+0.72}_{-0.24})$	–	$1.30\ (^{+0.55}_{-0.25})$
1500	[OII]	$1.11\ (^{+0.51}_{-0.19})$	$1.67\ (^{+0.68}_{-0.41})$	$1.13\ (^{+0.55}_{-0.20})$
2000	[OII]	$1.00\ (^{+0.40}_{-0.16})$	$1.44\ (^{+0.68}_{-0.32})$	$1.02\ (^{+0.43}_{-0.16})$
2500	[OII]	$0.93\ (^{+0.33}_{-0.14})$	$1.30\ (^{+0.68}_{-0.26})$	$0.95\ (^{+0.35}_{-0.14})$
3000	[OII]	$0.88\ (^{+0.29}_{-0.12})$	$1.19\ (^{+0.68}_{-0.22})$	$0.89\ (^{+0.30}_{-0.13})$
3500	[OII]	$0.83\ (^{+0.25}_{-0.11})$	$1.11\ (^{+0.56}_{-0.20})$	$0.84\ (^{+0.27}_{-0.12})$
4000	[OII]	$0.80\ (^{+0.23}_{-0.10})$	$1.05\ (^{+0.48}_{-0.17})$	$0.81\ (^{+0.24}_{-0.11})$
4500	[OII]	$0.77\ (^{+0.21}_{-0.09})$	$1.00\ (^{+0.42}_{-0.16})$	$0.78\ (^{+0.22}_{-0.10})$
5000	[OII]	$0.74\ (^{+0.19}_{-0.09})$	$0.95\ (^{+0.38}_{-0.15})$	$0.75\ (^{+0.20}_{-0.09})$
5500	[OII]	$0.72\ (^{+0.20}_{-0.084})$	$0.91\ (^{+0.35}_{-0.14})$	$0.73\ (^{+0.19}_{-0.09})$

the [OII] and [NII] measurements seem more close. On the other hand, the differences between [NII] temperature estimation in used density range is only $0.20{\cdot}10^4$ K, which is in the same order as the errors in [NII] temperature measurements. We can conclude that the electron temperature in knot-1 is in the range of $1.79(^{+0.21}_{-0.15})$ $\cdot 10^4$–$1.99(^{+0.25}_{-0.18})\cdot 10^4$ K, the lower temperature corresponding to $5.5{\cdot}10^3$ cm^{-3} density

and the higher temperature to $0.5 \cdot 10^3$ cm^{-3} density.

The energy source of a nova remnant can be photoionization from the central star and shock ionization, which is caused by ejecta running into interstellar medium in high velocity. Shock wave heats the gas to higher temperatures than photoionization (Osterbrock & Ferland 2006, p. 316-317). Nova Persei, as an energetic nova remnant, should have higher temperatures (several 10^4 K up to 10^5 K) than a pure photoionization-heated nebula (typically 10^4 K). The stellar remnant of Nova Persei is known to be a weak UV source (Evans et al. 1992), so the excitation is less likely be caused by photoionization. Results from the optical imaging study, given in Section 5.1, also proves shock-wave heating as remnant's heat source: shocks go together with highly supersonic velocities (mainly 600-1000 km/s) of knots. Additionally, forbidden lines can only be present in a spectrum of a remnant, if the temperatures are high and the density low. The spectrum of Nova Persei in the optical region consists of mainly forbidden lines. For example, the forbidden lines of nova remnant DQ Herculis 1934 disappeared with the expansion of the remnant, the electron temperature is estimated to be only 500 K (Osterbrock & Ferland 2006, p. 295-301).

6 Summary

The remnant of Nova Persei 1901 is one of the most energetic among known remnants. Unlike most astronomical objects, the evolution of GK Persei is observable even in monthly intervals using ground based telescopes and so makes an excellent research object. This Bachelor's thesis is part of an international study of the evolution of stellar outflow of Nova Persei 1901, which in turn is part of a project that studies the structure and kinematics of circumstellar matter around typical representatives of outbursting stellar objects. This thesis combines imaging and spectroscopy of Nova Persei's remnant to learn about the expansion of the optical remnant and about the current physical condition inside the gas clumps.

First, an optical imaging time-series of the remnant was put together from 19 observations using mainly The Isaac Newton Telescope with Wide Field Camera and Hα6568 narrowband filter and The Nordic Optical Telescope with ALFOSC instrument and Hα6577 filter. Five additional archival images from earlier observations were also used. The observations covered the time span of seven years (25 years with archival images). The acquired time series allowed us to measure the proper motions of 283 (from which the author of current Bachelor's thesis measured 110) and fluxes of 190 gas-clumps of the remnant. While the proper motions could be measured from all images, flux evolution could be measured only from flux-matched images, with the time span of seven years. The purpose of this Bachelor thesis was to perform measurements, which gave scientifically valuable data for the study of the evolution of stellar outflow of GK Persei and the results are published in Liimets et al. (2012), where velocities, kinematical ages, decelerations/accelerations, flux evolution and the apparent expansion of the nebula were found. In Liimets et al. (2012) proper motion measurements were combined with radial velocity measurements from spectroscopic data. We showed that the velocities of knots in the nova remnant's shell range from 250 to 1100 km/s (with the majority in the 600-1000 km/s range). The remnant is known to be highly asymmetric, but contrary to studies published before about GK Persei in different wavelengths (e.g Bode et al. (2004), Takei et al. (2015)), we did not find any evidence of uneven expansion in different directions of the remnant. The flux evolution measurements showed that half of the knots show consistent fading, others show constant flux (15%), constant brightening (20%) or fast change in flux (15%).

Secondly, emission line diagnostics was used to evaluate the electron temperatures of the knots. For this, long-slit spectrum of a part of the remnant of GK Persei was acquired with the Nordic Optical Telescope with ALFOSC instrument's spectrograph.

The task was to perform standard data reduction and calibration on the spectrum, to extract one-dimensional spectra of the knots and to analyse the emission line flux ratios using [OII]3726+3729, 7320+7330 (Å) and [NII]6548+6583, 5755 (Å) spectral lines. The spectrum of the knots is a typical nebular type spectrum with Hα and Hβ Balmer lines and strong [OIII], [OII], [NII] forbidden lines. The electron temperature calculations need certain emission line ratios and assumed density as input, we chose a range of densities $0.5{\cdot}10^3$–$5.5{\cdot}10^3$ cm^{-3}. [OII] line diagnostics gave lower, less precise temperatures (order of, mostly less than 10^4 K), due to the inhomogeneous light pollution and fringing pattern in the areas of the long-slit spectra, where necessary [OII] lines were situated. The more trustworthy results from [NII] line diagnostics gave the temperature in the range of $1.8{\cdot}10^4$–$2.0{\cdot}10^4$ K, the lower temperature corresponding to $5.5{\cdot}10^3$ cm^{-3} density and the higher temperature to $0.5{\cdot}10^3$ cm^{-3} density. As we found the velocities of knots being highly supersonic from the optical imaging time-series measurements, the remnant is shock-heated and so high temperatures are typical with shock-heated nebulae.

Noovajäänuki Nova Persei 1901 füüsikalised omadused

Kristiina Verro

7 Kokkuvõte

Nova Persei 1901 (ka GK Persei, GK Per) on klassikalise noova jäänuk. Valge kääbuse (primaartähe) ja hilistüüpi tähe (sekundaartähe) kaksiksüsteemis toimus aine ülevool sekundaartähelt valgele kääbusele. Viimase pinnal tõusis temperatuur, kuni jõudis 10^7 K suurusjärguni, mil algasid hetkelised termotuumareaktsioonid. Plahvatusliku protsessi käigus visati valge kääbuse ümber olev aine süsteemist välja, millest tekkis noovajäänuk kaksiktähe ümber.

Nova Persei 1901 plahvatas 1901. aastal ning noovajäänuk sai vaadeldavaks 15 aastat hiljem. Tegemist on väga energiarikka noovajäänukiga, mille evolutsioon on vaadeldav maapealsete teleskoopidega juba kuude lõikes. Seesugune meile näiv kiire noovajäänuki areng annab suurepärase võimaluse saada vastuseid noovajäänuki kui udukogu struktuuri ja kinemaatika kohta. Antud bakalaureusetöö on osa rahvusvahelisest projektist (mille eestvedajaks on R. Corradi), mis uurib tüüpiliste ainet väljapaiskavate tähtede (R Aquarii, V838 Monocerotis, Nova Persei 1901) jäänukeid. Kuigi tähed ise on sümmeetrilised, pole seda tihti noovajäänukid, ka mitte Nova Persei. Algsed ülesvõtted optilises lainealas näitasid ainet vaid kaksiktähest edelaosas; ka teistes lainealades on vaadeldud ebasümmeetrilist jäänukit, mille heleduse maksimum asub edelaosas (näiteks Bode et al. (2004), Takei et al. (2015)), kuid praegused vaatlusandmed optilises lainealas näitavad sümmeetrilist jäänukit.

2004. aastast kuni 2011. aastani vaadeldi Nova Perseid Isaac Newtoni teleskoobi ja Põhjamaade optilise teleskoobiga, sarnastes Hα filtrites. Lisati ka viis arhiivipilti varasematest aastatest. Kui 19 vaatlust tehti seitsme aastase ajaintervalli sees, siis koos arhiivipiltidega kaeti noovajäänuki 25 aastane evolutsioon. Antud bakalaureusetöö eesmärgiks oli mõõta nendelt piltidelt noovajäänuki gaasiklompide omaliikumist ehk liikumist taevatasandil. Kuna 15 kaadrit oli tehtud sama Isaac Newtoni teleskoobi, instrumendi ja filtriga, olid need kaadrid suhtelistes heleduste ühikutes võrreldavad. Käesoleva bakalaureusetöö eesmärgiks oli ka mõõta apertuurfotomeetria abil gaasiklompide heledused igal kaadril (v.a 1999. aasta kaadrilt), kus klomp oli vaadeldav, et saada andmeid heleduse evolutsiooni analüüsiks. Omaliikumiste ja heleduste mõõtmised tehti Liimets et al. (2012) artikli tarbeks, kus mõõtmiste põhjal leiti gaasiklompide kiirused, kinemaatilised vanused, heleduse evolutsioon ja

noovajäänuki üldine näiv paisumine. Tähtsaim tulemus on üllatav – me ei leidnud tõendeid ebaühtlase paisumise kohta, ka mitte edelasuunas.

Bakalaureusetöö teiseks eesmärgiks oli kasutada 2007. aastal Põhjamaade optilise teleskoobiga (instrumendiga ALFOSC) tehtud pikapilu spektrit noovajäänuki läbilõikest, millele jäid 10 gaasiklompi, et saada gaasiklompide sisene elektrontemperatuuri hinnang. Elektrontemperatuur on koos elektrontihedusega jäänuki tähtsaim siseparameeter, mis vihjab ka jäänukis valitsevale energiaallikale, milleks võib olla UV fotoionisatsioon või põrkeionisatsioon. Enne klombisisese temperatuuri analüüsi, viidi läbi põhjalik standardne andmetöötlus, kalibreeriti peale lainepikkuste ja kiirgustiheduse skaala ning eraldati kahedimensionaalsest spektrist ühedimensionaalsed gaasiklompide spektrid. Noovajäänuki spekter on emissioonispekter. Heledaima pilule jäänud gaasiklombi spektris oli 14 emissioonijoont: vesiniku Hα ja Hβ ning nn keelatud jooned [OIII], [OII], [OI] [NII] ja [NeIII]. Elektrontemperatuuri saab hinnata teatud emissioonijoonte intensiivsuste suhete järgi, milleks meie spektris olid [OII] jooned 3726+3729 Å ja 7320+7330 Å ning [NII] jooned 6548+6583 Å ja 5755 Å. Temperatuuri arvutusteks eeldasime eletrontiheduse vahemikku $0.5{\cdot}10^3$–$5.5{\cdot}10^3$ cm^{-3}. [OII] emissioonijoonte baasil tehtud arvutused andsid laiema temperatuuride vahemiku ning madalamad temperatuurid kui [NII] joontel põhinevad arvutused. [OII] joonte intensiivsuste mõõtmine ja arvutusteks kasutamine oli ebatäpsem, kuna jooned asusid üksteisest kaugel ning spektri mürases piirkonnas. Tulemused olid suurusjärgus 10^4 K. [NII] joonte intensiivsuste mõõtmine oli täpsem, kuna spektrijooned asusid spektris lähestikku ning spektri keskel. Temperatuuriks saime $1.8{\cdot}10^4$–$2.0{\cdot}10^4$ K, kus madalam temperatuur vastab elektrontihedusele $5.5{\cdot}10^3$ cm^{-3} ja kõrgem temperatuur vastab tihedusele $0.5{\cdot}10^3$ cm^{-3}. [NII] joonte põhjal saadud temperatuuri hinnangut toetab ka teooria. Gaasiklompide kiirused on suurelt üle helikiiruse, millega kaasnevad lööklained, põrkeionisatsioon ja kõrgem temperatuur ([NII] temperatuuride suurusjärgus). Nova Persei on nõrk UV kiirgaja, seega pole ilmselt noovajäänukis peamiseks energiaallikaks fotoionisatsioon, millega kaasneksid madalamad temperatuuride suurusjärgud ([OII] joonte analüüsist saadud temperatuuride suurusjärk). Seega valitseb noovajäänukis põrkeionisatsioon ja gaasiklompide sees on temperatuurid ligikaudu $1.9{\cdot}10^4$ K.

8 References

Barnard F.A.P., 1916, Nebulosity around Nova Persei, Harvard College Observatory Bulletin vol. 621, 1–1

Bode M.F., O'Brien T.J., Simpson M., 2004, Echoes of an Explosive Past: Solving the Mystery of the First Superluminal Source, Astrophys. J. vol. 600, L63–L66

Chromey F.R., 2010, To Measure the Sky, Cambridge University Press

Corradi R.L.M., 2014, (Direct) determination of physical and chemical conditions from optical spectra, lecture slides for Advanced School: "The interaction of stars with the interstellar medium of galaxies"

De Robertis M.M., Dufour R.J., Hunt R.W., 1987, A five-level program for ions of astrophysical interest, JRASCvol. 81, 195–220

Emerson D., 1997, Interpreting Astronomical Spectra, John Wiley and Sons

Evans A., Bode M.F., Duerbeck H.W., Seitter W.C., 1992, IUE observations of the shells of RR PIC and GK Per, Mon. Not. R. Astron. Soc. vol. 258, 7P–13P

Fitzpatrick E.L., Massa D., 2009, An Analysis of the Shapes of Interstellar Extinction Curves. VI. The Near-IR Extinction Law, Astrophys. J. vol. 699, 1209–1222

Liimets T., Corradi R.L.M., Santander-García M., Villaver E., Rodríguez-Gil P., Verro K., Kolka I., 2012, A Three-dimensional View of the Remnant of Nova Persei 1901 (GK Per), Astrophys. J. vol. 761, 34

Massey P., 1997, A User's Guide to CCD Reductions with IRAF

Mathis J.S., 1990, Interstellar dust and extinction, ARA&Avol. 28, 37–70

Moore P., Rees R., 2011, Patrick Moore's Data Book of Astronomy, Cambridge University Press

Osterbrock A.E., Ferland G.J., 2006, Astrophysics of Gaseous Nebulae and Active Galactic Nuclei

Pickering E.C., 1901, Anderson's New Star in Perseus., Harvard College Observatory Circular vol. 56, 1–4

Shara M.M., Zurek D., De Marco O., Mizusawa T., Williams R., Livio M., 2012, GK Per (Nova Persei 1901): Hubble Space Telescope Imagery and Spectroscopy of the Ejecta, and First Spectrum of the Jet-like Feature, Astronomical Journalvol. 143, 143

Shaw R.A., Dufour R.J., 1995, Software for the Analysis of Emission Line Nebulae, Pub. Astron. Soc. Pacific vol. 107, 896

Takei D., Drake J.J., Yamaguchi H., Slane P., Uchiyama Y., Katsuda S., 2015, X-Ray Fading and Expansion in the "miniature Supernova Remnant" of Gk Persei, Astrophys. J. vol. 801, 92

Tweedy R.W., 1995, Nova Persei 1901: Detection of the site of its brightest light echo, Astrophys. J. vol. 438, 917–920

Wu C.C., Holm A.V., Panek R.J., Raymond J.C., Hartmann L.W., Swank J.H., 1989, Ultraviolet spectrophotometry and optical and infrared photometry of the old nova GK Persei, Astrophys. J. vol. 339, 443–454

9 Acknowledgements

My deepest expression of appreciation goes to Tiina Liimets from Tartu Observatory, who not only acted as the primary supervisor for my thesis, but also as the guide in the world of science. She taught me observational astronomy starting from observations, finishing with data analysing. From day one she provided me with opportunities and contacts in the national and international scale.
I want to thank my supervisor Romano Corradi from The Instituto de Astrofísica de Canarias, who took the time to teach me about the nuances of data reduction and calibration and who checked and advised my work at every stage.
I am grateful for the staff of Tartu Observatory for the inspiring and supportive work environment. Among them, special thanks to Indrek Kolka and Tõnis Eenmäe, who often gave me advice, ideas and guidelines.

10 Appendix

10.1 First Appendix

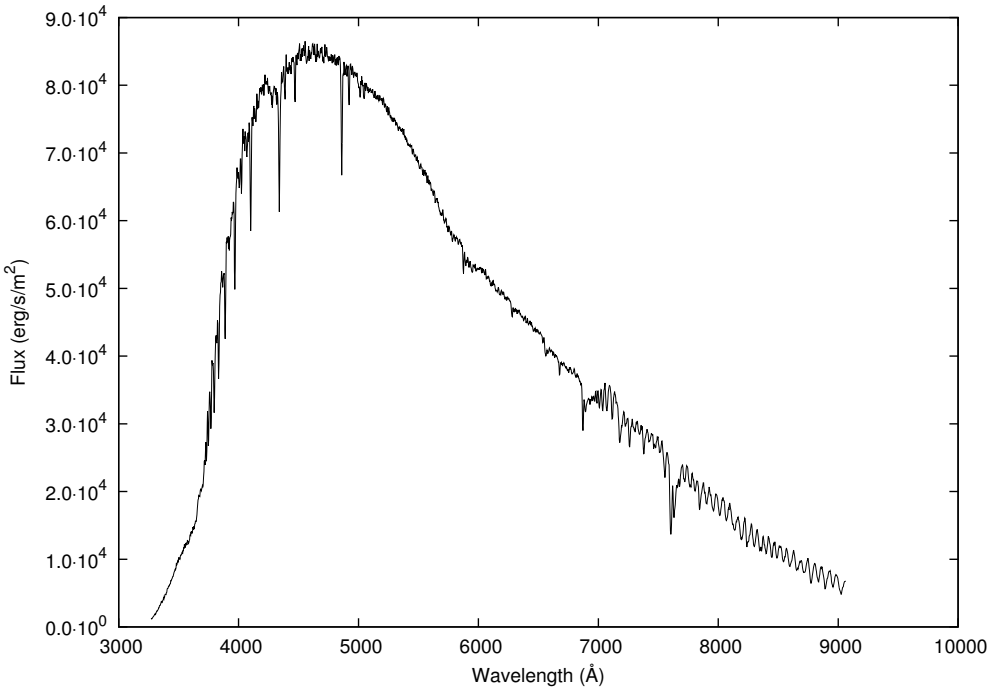

Figure 9: Spectrum of the standard star BD+332642

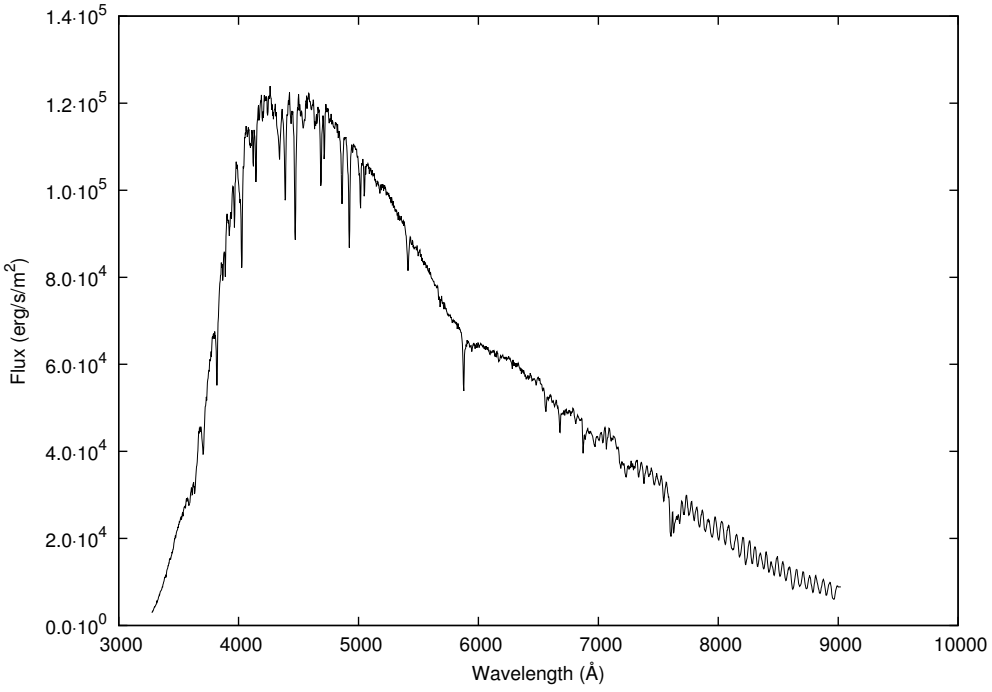

Figure 10: Spectrum of the standard star BD+254655

10.2 Second Appendix

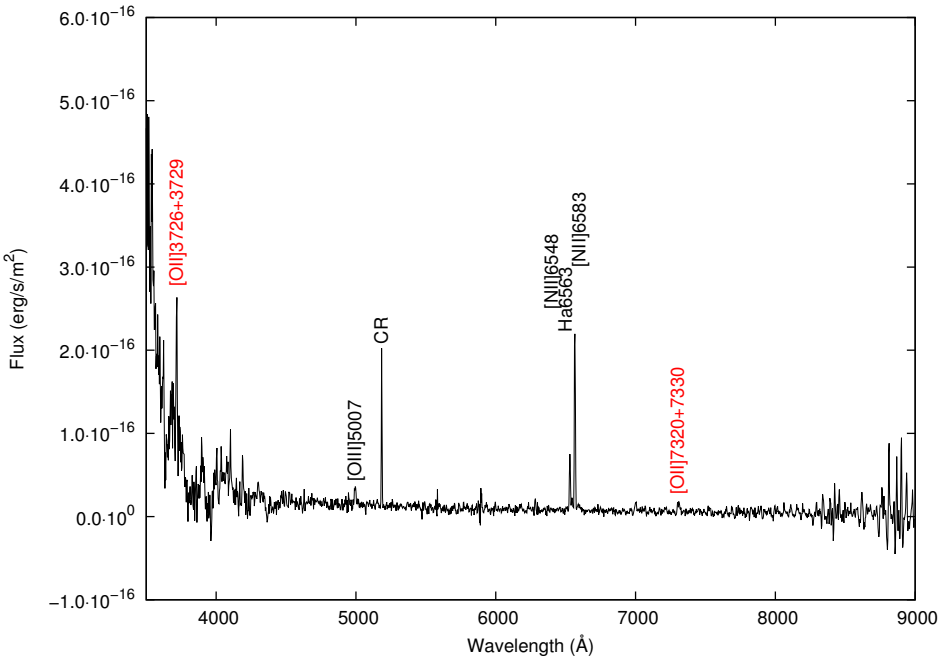

Figure 11: One-dimensional spectrum of knot-2. Problematic background flux can be seen in the blue and fringing pattern in the red wavelengths. Emission lines used in temperature estimation are marked with red ([OII]).

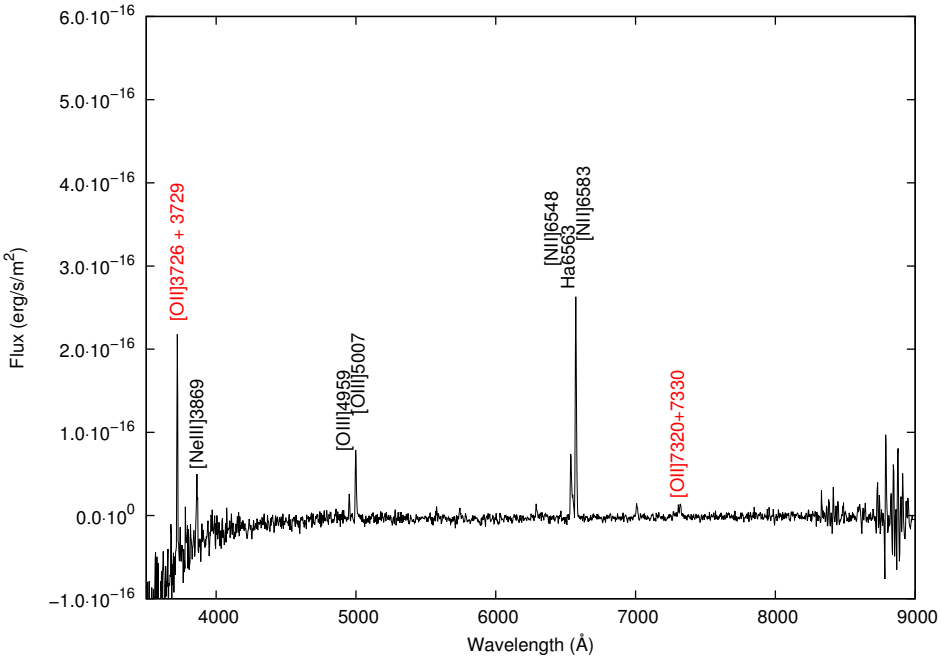

Figure 12: One-dimensional spectrum of knot-3. Problematic background flux can be seen in the blue and fringing pattern in the red wavelengths. Emission lines used in temperature estimation are marked with red ([OII]).

10.3 Third Appendix

```
import math
import fileinput
import numpy as np

#file with spectral lines, zero column lambda, second column
   flux:
spec=[line.strip() for line in open("knot1.txt", 'r')]
#correction file, zero column lambda, first curve:
corr=[line.strip() for line in open("Correctionfile.txt", 'r')]

for i in spec:
    if len(i) and i[0] == '#':  #, len is length, first letter,
       takes hashtag lines out
        continue
    veerud_spec=i.split()
#the closest lambda from correction file:
    kaugus=0
    indeks=(-5)
    for j in corr:
        veerud_corr=j.split()
        if indeks == -5:
            kaugus=abs(float(veerud_spec[0])-float(veerud_corr
               [0]))
            indeks=veerud_corr
            continue
        if abs(float(veerud_spec[0])-float(veerud_corr[0])) <
           kaugus:
            kaugus=abs(float(veerud_spec[0])-float(veerud_corr
               [0]))
            indeks=veerud_corr
            continue
#second closest:
    kaugus2=0
    indeks2=-5
    for j in corr:
        veerud_corr=j.split()
        if kaugus==abs(float(veerud_spec[0])-float(veerud_corr
           [0])):
            continue
```

```
    if indeks2 == -5:
        kaugus2=abs(float(veerud_spec[0])-float(veerud_corr
            [0]))
        indeks2=veerud_corr
        continue
    if abs(float(veerud_spec[0])-float(veerud_corr[0])) <
       kaugus2:
        kaugus2=abs(float(veerud_spec[0])-float(veerud_corr
            [0]))
        indeks2=veerud_corr
        continue
a=float(indeks[1]) #closest correction
b=float(indeks2[1]) #second closest correction
c=float(indeks[0]) #closest lambda
d=float(indeks2[0]) #second closest lambda
e=float(veerud_spec[0])
if c>d:
    alambda=(b-((b-a)/(c-d))*(e-d)) #right correction
else:
    alambda=(a-((a-b)/(d-c))*(e-c)) #right correction
Cb=0.323  #logarithmic extinction at H-beta
Rv=3 #selective extinction ratios
flambda= 0.84789 * (1+((alambda)/3)) # normalized extinction
    function
flux_uus=float(veerud_spec[2])*pow(10,Cb*flambda) #
   extinction law
print(flux_uus)
```

Lihtlitsents lõputöö reprodutseerimiseks ja lõputöö üldsusele kättesaadavaks tegemiseks

Mina, Kristiina Verro,

1. annan Tartu Ülikoolile tasuta loa (lihtlitsentsi) enda loodud teose
„Physical Properties of the Nova Remnant Nova Persei 1901”

mille juhendajateks on
Tiina Liimets ja Romano L. M. Corradi,

1.1. reprodutseerimiseks säilitamise ja üldsusele kättesaadavaks tegemise eesmärgil, sealhulgas digitaalarhiivi DSpace-is lisamise eesmärgil kuni autoriõiguse kehtivuse tähtaja lõppemiseni;
1.2. üldsusele kättesaadavaks tegemiseks Tartu Ülikooli veebikeskkonna kaudu, sealhulgas digitaalarhiivi DSpace´i kaudu kuni autoriõiguse kehtivuse tähtaja lõppemiseni.

2. olen teadlik, et punktis 1 nimetatud õigused jäävad alles ka autorile.

3. kinnitan, et lihtlitsentsi andmisega ei rikuta teiste isikute intellektuaalomandi ega isikuandmete kaitse seadusest tulenevaid õigusi.

Tartus, **20.05.2015**